中國機械工程學刊第四十六卷第四期第 387~396 頁(民國一百一十四年)
Journal of the Chinese Society of Mechanical Engineers, Vol.46, No.4, pp387~396 (2025)

Enhanced and Optimized Thermoelectric Efficiency of SOFC-Based Hybrid Power Generation Systems

Ciao-Lun Huang*, Hsin-Yi Lai* and Yen-Hsin Chan**

Keywords: Solid oxide fuel cell; hybrid power generation system; exergy analysis; Reformer

ABSTRACT

This study focuses on the hybrid power generation system of Solid Oxide Fuel Cells (SOFC), investigating the impact of integrating different types of external combustion engines (Gas turbine, Organic Rankine cycle, and Stirling engine) on system thermoelectric efficiency after selecting an appropriate reformer. By analyzing the thermoelectric efficiency differences of SOFC systems combined with three types of external combustion engines under various fuel utilization rates, the study evaluates the irreversible energy losses in each component based on the principles of entropy generation and exergy analysis.

Numerical simulations of energy and mass transfer reveal that, both qualitatively and quantitatively, the SOFC-SE configuration achieves the highest system thermoelectric efficiency. Entropy generation and exergy calculations indicate that the SOFC-ORC hybrid system exhibits the highest entropy generation, resulting in comparatively lower efficiency. In contrast, the SOFC-SE hybrid system demonstrates superior exergy efficiency. Factors such as temperature differences at component inlets and outlets, chemical reactions, and external heat transfer significantly influence entropy generation.

INTRODUCTION

Due to the current global issue of energy shortages, the development of renewable energy has gained increasing attention, particularly in fuel cells, wind power, and solar cells. Fuel cells generate electricity by introducing oxygen (air) at the cathode, allowing oxygen ions to pass through the electrolyte layer to the anode and react with hydrogen. The only byproduct is water. Among various types of fuel cells, solid oxide fuel cells (SOFCs) offer advantages such as high fuel utilization, high efficiency, long-term stability, and fuel flexibility (Somekawa et al. 2017, Vrečko et al. 2018, Liso et al. 2011).

SOFCs can operate with various fuels, including hydrocarbons (e.g., methane, ethanol) and hydrogen. However, hydrocarbon fuels are often impure, leading to lower system efficiency. Direct feeding of hydrocarbonsinto the stack may cause carbon deposition. To address this, SOFC systems typically employ a reformer to convert most hydrocarbons into hydrogen before delivering them to the stack. Therefore, the successful commercialization of SOFC systems may rely on the ability to convert available fuels into H_2 and CO (Lai et al. 2025, Bae et al. 2010). In addition to these advantages, SOFC systems produce high-temperature exhaust gases, which, according to many studies, can be utilized effectively by integrating SOFCs with external combustion engine systems.

Three primary reforming methods are commonly used: steam reforming (SR), partial oxidation (POx), and autothermal reforming (ATR) (Somekawa et al. 2017, Liso et al. 2011, Vita et al. 2019). Among them, SR offers a high hydrogen yield and enables high SOFC output power. However, the endothermic nature of the reaction requires high-temperature operation and stringent thermal management. POx, an exothermic reaction, can operate without external heat sources and enables rapid startup but provides a significantly lower hydrogen yield, resulting in lower SOFC output power (Liso et al. 2011).

ATR combines both SR and POx reactions by co-feeding hydrocarbons, steam, and air into the reformer. The feed composition can be adjusted to maintain a slightly exothermic reaction. Compared to SR, ATR allows faster startup and requires a simpler system structure, while offering higher hydrogen production and greater output power than POx. Among the three, ATR achieves the highest methane conversion rate, effectively combining the benefits of

Paper Received January, 2025. Revised March, 2025. Accepted April, 2025. Author for Correspondence: Yen-Hsin Chan.

* *Student, Department of Mechanical Engineering, National Cheng Kung University Tainan, Taiwan, R.O.C..*
** *Professor, Department of Mechanical Engineering, National Cheng Kung University Tainan, Taiwan, R.O.C..*
*** *Professor, Department of Mechanical and Computer-Aided Engineering, Feng Chia University Taichung, Taiwan, R.O.C..*

SR and POx. Since each reforming method involves different control parameters, the system requires corresponding loop designs, which in turn affect system efficiency. Proper selection of reformer type and operating conditions is therefore crucial for system performance. However, few studies have investigated SOFC systems with external ATR reformers. This study aims to compare system loop designs and operating parameters under three reforming methods, and to improve system power output and efficiency.

Given that SOFCs produce high-temperature exhaust gases during power generation, these gases can be utilized in hybrid systems with various external engines. Without proper handling, the exhaust can cause thermal damage to the environment and cannot be directly reused. Therefore, integrating external combustion engines to enhance system efficiency demands effective thermal management to maintain high-temperature operation. Previous studies have suggested discharging excess water from the system to raise system temperature (Somekawa et al. 2017). The most commonly considered external engines for integration with SOFCs include gas turbines (GT), Stirling engines (SE), and organic Rankine cycles (ORC).

This study employs entropy generation-based thermodynamic analysis to evaluate entropy generation in each system component. Rather than focusing on the performance of individual components, the study accounts for energy losses and optimal operating conditions of all components. For complex hybrid systems composed of multiple subsystems, thermal control plays a critical role in thermal analysis. Optimization of key components such as the SOFC stack and external engine is also conducted. The fuel utilization rate in the SOFC stack significantly influences SOFC efficiency and system temperature, while the compression ratio is the key parameter affecting external engine efficiency.

The objective of this study is to investigate the influence of different reformers on system power output and efficiency. The effects of operating parameters for ATR, SR, and CPOx reformers on component temperatures, output power, and efficiency are evaluated. Furthermore, the study explores performance enhancement and optimization of systems integrated with different external engines, including (1) gas turbines, (2) organic Rankine cycles, and (3) Stirling engines, under varying operating parameters. Finally, entropy generation and exergy analysis are applied to examine thermodynamic irreversibility of system components and compare the exergy efficiency of the overall system.

Modeling Methodology

Modeling of the SOFC

In the power generation process of SOFCs, electrochemical reactions between air and fuel are utilized to produce electricity. Oxygen flows along the cathode, and when oxygen molecules reach the cathode/electrolyte interface, they gain four electrons from the cathode and dissociate into two oxide ions. The electrochemical reaction occurring at the cathode is as follows:

$$O_2 + 4e^- \rightarrow 2O^{2-} \quad (1)$$

The oxide ions diffuse through the electrolyte material and migrate to the anode side of the cell. These oxide ions pass through the porous electrolyte and react with hydrogen (fuel) to produce water. A commonly used fuel is natural gas, which is processed through desulfurization, reforming, and conversion to obtain hydrogen. A detailed discussion will be provided in the next subsection. The electrochemical reaction occurring at the anode is as follows:

$$2H_2 + 4O^{2-} \rightarrow H_2O + 4e^- \quad (2)$$

The electrons are transported from the anode to the external circuit and return to the cathode, generating an electromotive force (EMF) between the two electrodes. By connecting the electrodes through an external circuit, electric current can be produced. The overall electrochemical reaction is as follows:

$$H_2 + \frac{1}{2}O_2 \rightarrow 2H_2O \quad (3)$$

When methane is used as the fuel, CH_4 reacts with O_2 through an internal reformer to produce H_2O and CO_2. The overall reaction is as follows:

$$CH_4 + 2O_2 \rightarrow 2H_2O + CO_2 \quad (4)$$

SOFC generates electricity by converting chemical energy into electrical energy through the aforementioned electrochemical reactions. Gibbs free energy represents the usable energy of a system at constant temperature, excluding energy lost as heat to the surroundings. The electromotive force (EMF) obtained from SOFC can be evaluated by the change in Gibbs free energy (ΔG), which is the difference between the products and reactants, as shown below:

$$\Delta G = \Delta G_{products} - \Delta G_{reactants} \quad (5)$$

Considering the thermodynamic characteristics of a reversible process:

$$dG = VdP - SdT \quad (6)$$

Among them, V denotes volume, P is the operating pressure, and T is the operating temperature. Assuming an isothermal process, substituting the ideal gas equation PV = nRT into the above expression yields:

$$dG = nRT\, dP/P \quad (7)$$

Where R is the ideal gas constant and nnn is the number of moles. For the reaction aA+bB→mM+nN under isothermal and isobaric conditions, introducing the standard Gibbs free energy (ΔG_0) at standard pressure, integration of the above expression yields:

$$\Delta G = \Delta G_0 + RT \ln\left(\frac{P_M^m P_N^n}{P_A^a P_B^b}\right) \quad (8)$$

Where A and B are the products, M and N are the reactants, a and b are the mole numbers of the products, and m and n are the mole numbers of the reactants. Using methane as the fuel as an example:

$$\Delta G = \Delta G_0 + RT \ln\left(\frac{P_{CH_4} P_{O_2}^2}{P_{H_2O}^2 P_{CO_2}}\right) \quad (9)$$

The relationship between the electromotive force of the fuel cell and the Gibbs free energy is expressed as:

$$E = \frac{\Delta G}{n_e F} \quad (10)$$

Where E is the electromotive force, $n_e$is the number of electrons transferred through the external circuit per fuel molecule, and F is the Faraday constant. Substituting equation (9) into equation (10) yields the Nernst equation:

$$E = \frac{\Delta G_0}{n_e F} + \frac{RT}{n_e F} \ln\left(\frac{P_M^m P_N^n}{P_A^a P_B^b}\right) \quad (11)$$

For SOFCs using hydrogen as fuel, the expression for the electromotive force (V_{OCV}) is given as:

$$V_{OCV} = V_0 + \frac{RT}{2F} ln \frac{P_{H_2} P_{O_2}}{P_{H_2O}} \quad (12)$$

Where V_0 is the ideal voltage under standard pressure conditions (Duc and Fujit 2012).

The derived potential represents a reversible and ideal open circuit voltage (OCV). However, practical fuel cells are neither reversible nor ideal, thus the overpotential resulting from irreversibility must be considered. The major polarization losses in fuel cells can be categorized into three types: ohmic polarization, activation polarization, and concentration polarization (Lai et al. 2025).

Ohmic polarization, also referred to as ohmic overpotential or ohmic losses, arises from the electrical resistance to ion transport (through the electrolyte) and electron transport (through the electrodes and current collectors), as well as contact resistance between cell components (Aguiar et al. 2004). When electrons and ions pass through electronic and ionic conductors, respectively, under fixed temperature and geometry, the voltage loss is proportional to the current and follows Ohm's law. Therefore, the total ohmic overpotential can be expressed as:

$$\eta_{Ohm} = iR_{Ohm} \quad (13)$$

Where i is the current density and $R_{Ohm}$is the internal resistance of the cell (including both electronic and ionic resistances). R_{Ohm} primarily originates from the cathode, anode, and electrolyte, and can be determined based on the relationship between their thickness and conductivity as follows:

$$R_{Ohm} = \frac{\tau_{anode}}{\sigma_{anode}} + \frac{\tau_{electrolyte}}{\sigma_{electrolyte}} + \frac{\tau_{cathode}}{\sigma_{acthode}} \quad (14)$$

σ is the electrical conductivity of electrons and ions (Duc and Fujit 2012).

Activation polarization results from the need to overcome the activation energy barrier before the chemical reaction occurs, leading to a voltage drop due to the sluggish reaction at the electrode–electrolyte interface. At higher operating temperatures, electrode reactions proceed rapidly, making activation polarization relatively small; however, as the operating temperature decreases, activation polarization may become the dominant cause of voltage loss (Lai et al. 2025).

$$\eta_{act} = \eta_{act,a} + \eta_{act,c} \quad (15)$$

$$\eta_{act,a} = \frac{RT}{F} \times \sinh^{-1}\left(\frac{i}{2i_{0,a}}\right) \quad (16)$$

$$\eta_{act,c} = \frac{RT}{F} \times \sinh^{-1}\left(\frac{i}{2i_{0,c}}\right) \quad (17)$$

Where$i_{0,a}$ and $i_{0,c}$are the exchange current densities of the electrodes, which are key parameters in activation polarization and are primarily influenced by operating pressure.

$$i_{0,a} = k_a \left(\frac{P_{H_2}}{P_{\text{ref}}}\right)\left(\frac{P_{H_2O}}{P_{\text{ref}}}\right) exp\left(-\frac{E_{act,a}}{RT}\right) \quad (18)$$

$$i_{0,c} = k_c \left(\frac{P_{O_2}}{P_{\text{ref}}}\right)^{0.25} exp\left(-\frac{E_{act,c}}{RT}\right) \quad (19)$$

Where $P_{\text{ref}}$is the reference pressure ($P_{\text{ref}} = 1$), k_a and k_c are the pre-exponential factors of the exchange current densities, $E_{act,a}$ and $E_{act,c}$ Eact,c are the activation energies of the exchange current densities.

Concentration polarization arises when mass transport limitations hinder the electrode reactions. When the flux of reactants entering and the flux of products exiting the electrode are slower than the reaction flux corresponding to the discharge current, a concentration gradient forms on the electrode, leading to concentration polarization. The physical processes involved include molecular diffusion of gas species within the electrode pores, dissolution of reactants into the electrolyte, dissolution of products from the electrolyte, and diffusion of reactants/products through the electrolyte during the reaction. For anode-supported PEN structures, concentration overpotential is typically minimal at the cathode but may become significant at the anode, especially under conditions of high current density and high fuel utilization. Concentration polarization is generally influenced by the diffusion coefficient (DDD), microstructure, partial pressure, and current density; therefore, the concentration overpotential in this study is determined using an empirical correlation:

$$\eta_{conc} = \eta_{conc,a} + \eta_{conc,c} \quad (20)$$

$$\eta_{conc,a} = \frac{RT}{2F} \ln\left(\frac{P_{H_2}}{P_{H_2,TPB}} \frac{P_{H_2O,TPB}}{P_{H_2O}}\right) \quad (21)$$

$$\eta_{conc,c} = \frac{RT}{4F} \ln\left(\frac{P_{O_2}}{P_{O_2,TPB}}\right) \quad (22)$$

Where $P_{H_2,TPB}$, $P_{H_2O,TPB}$and $P_{O_2,TPB}$ are the partial pressures of each gas species at the three-phase boundary (TPB) layer, which can be calculated using the following equations:

$$P_{H_2,TPB} = P_{H_2} - \frac{t_a \cdot i \cdot RT}{2F \cdot D_{a,eff} \cdot P} \quad (23)$$

Based on the overall reaction of the SOFC stack (Eq. 3), the variations in energy and flow rate can be determined, allowing the calculation of inlet and outlet temperatures at the cathode and anode of the stack. In general, SOFCs do not completely consume hydrogen; that is, the fuel utilization rate of the stack is not 100%. The remaining fuel is directed to a burner for complete combustion, ensuring full utilization of the fuel supplied to the power

generation system while also serving as a heat source to maintain high system temperatures. The fuel utilization rate of the stack can be expressed as:

$$FU = \frac{\dot{n}_{fuel,react}}{\dot{m}_{fuel,in}} = \frac{N_C \cdot I \cdot V_N \cdot 60}{n_e \cdot F \cdot (\dot{V}_{H2} + \dot{V}_{CO} + 4\dot{V}_{CH4})} \quad (24)$$

Where $\dot{V}$ is the fuel flow rate (Nl/min), N_C is the number of single cells, n_e is the number of electrons, III is the current (A), and V_N is the molar volume ($V_N = 24.5Nl/mol$).

Based on the aforementioned calculation methods for SOFC, single-cell simulations can be conducted to obtain the polarization curve. Table 1 lists the parameters for the operating conditions of SOFC (Noponen et al. 2015) and calculations are performed at operating temperatures of 973 K, 1023 K, and 1073 K, respectively.

Table 1. Operating parameters of the SOFC system (Noponen et al. 2015)

SOFC	
Parameters	Value
Number of cell [-]	200
Stack area [m^2]	2.42
Operating temperature [K]	973-1073
Operating pressure [bar]	1-5
Thickness of electrolyte [m]	3×10^{-6}
Thickness of anode [m]	400×10^{-6}
Thickness of cathode [m]	12×10^{-6}
σ_e [-]	$33.4\times10^3 \times exp\left(\frac{-10300}{T}\right)$
σ_a [-]	$\frac{95\times10^6}{T} \times exp\left(\frac{-1150}{T}\right)$
σ_c [-]	$2.45\times10^5 \times exp\left(\frac{-97.5}{T}\right)$
$D_{a,eff}$ [m^2/s]	3.66×10^{-5} (m^2/s)
$D_{c,eff}$ [m^2/s]	1.37×10^{-5} (m^2/s)
$E_{act,a}$[KJ /mole]	110(KJ /mole)
$E_{act,c}$[KJ /mole]	100(KJ /mole)
k_a[-]	3.621×10^9
k_c[-]	1.325×10^{10}

Modeling of the heat components

Due to the requirement for incorporating thermal components such as the SOFC stack, heat exchangers, reformer, and burner within the SOFC system, strong coupling exists among these components. Therefore, it is essential to understand the operating processes and principles of each system component, followed by conducting a thermodynamic analysis to investigate the thermal balance of each component within the system.

Heat exchanger

Due to the high-temperature nature of the SOFC power generation system and the requirement for maintaining the SOFC within a specific temperature range for operation, heat exchangers are commonly employed to recover and reutilize the high temperature and high energy released from system components. The following introduces the heat exchanger with the ε-NTU method, where the heat exchanger effectiveness is defined as follows:

$$\varepsilon = \frac{q}{q_{max}} \quad (25)$$

Where q represents the actual heat transfer rate, and q_{max} denotes the maximum possible heat transfer rate. The value of q_{max} can be calculated using the following equation:

$$q_{max} = C_{min}(T_{h,i} - T_{c,i}) \quad (26)$$

In the above equation, $T_{h,i}$ represents the inlet temperature of the higher-temperature fluid, $T_{c,i}$ represents the inlet temperature of the lower-temperature fluid, and C is the heat capacity rate, which is calculated as:

$$\begin{cases} C_c = \sum \dot{m}_c \, C_{p,c} \\ C_h = \sum \dot{m}_h \, C_{p,h} \end{cases} \quad (27)$$

C_{min} refers to the smaller value between C_c and C_h calculated from the above equation.

Finally, by substituting equations (26) and (27) into equation (25), the following relationship can be obtained:

$$\varepsilon = \frac{C_h(T_{h,i} - T_{h,o})}{C_{min}(T_{h,i} - T_{c,i})} = \frac{C_c(T_{c,o} - T_{c,i})}{C_{min}(T_{h,i} - T_{c,i})} \quad (28)$$

The relationship derived above can be used to determine the key operating parameters of the heat exchanger.

Reformer

The primary function of the reformer is to convert hydrocarbon fuels into CO and H_2, which can be utilized by the SOFC stack. The most common reforming methods include steam reforming (SR), partial oxidation reforming (POx), and autothermal reforming (ATR). Each of these methods exhibits different thermal characteristics, either endothermic or exothermic, and therefore has an optimal system configuration and parameter design. Detailed explanations of the chemical reaction equations and thermal changes will be provided in the next section.

For steam reforming, assuming complete conversion of the feed into hydrogen, the reforming reaction is given as follows (Carapellucci and Giordano 2020):

$$CH_4 + H_2O \rightarrow CO + 3H_2 \qquad \Delta H = 206(\tfrac{KJ}{mol}) \quad (29)$$

$$CO + H_2O \rightarrow CO_2 + H_2 \qquad \Delta H = -41(\tfrac{KJ}{mol}) \quad (30)$$

ATR [11] combines the steam reforming reaction with partial oxidation. A representative reaction equation for Atr is given as follows (Li et al. 2008):

$$CH_4 + 0.5O_2 \rightarrow CO + 2H_2 \quad H = -36(\tfrac{KJ}{mol}) \quad (31)$$

Based on the reaction equations, the heat required for the reforming process can be determined, allowing the outlet temperature of the reformer to be estimated. Additionally, the changes in reactants and products in the reaction indicate the variation in flow rates at the inlet and outlet of the reformer. Furthermore, the reformer is typically coupled with a suitable heat exchanger.

Burner

The burner is the primary component

responsible for supplying heat to the SOFC system. Since the SOFC stack does not fully consume all of the fuel, the remaining high-temperature fuel is directed to the burner for combustion. The high-temperature gas produced from this process is then transferred through a heat exchanger to preheat the inlet gases of the system, ensuring that the gases reach the required operating temperature for the stack. The combustion reaction and associated heat release are given as follows:

$$CH_4 + 2O_2 \rightarrow CO_2 + 2H_2O \quad \Delta H = 55500(\frac{KJ}{kg}) \quad (32)$$

$$\mathrm{CO} + 0.5O_2 \rightarrow CO_2 \qquad \Delta H = 1060(\frac{KJ}{kg}) \quad (33)$$

$$H_2 + 0.5O_2 \rightarrow H_2O \qquad \Delta H = 141700(\frac{KJ}{kg}) \quad (34)$$

Electrical and thermal efficiency of the SOFC power generation system

Based on the above, the calculations for all thermal components have been described. The following section presents the efficiency calculation of the SOFC system used in this study. System performance is evaluated primarily based on the first-law thermodynamic efficiency, calculated using the following equation:

$$\eta_{\mathrm{I}} = \frac{W_{\mathrm{sys}}}{q_{\mathrm{fuel,in}} \times \mathrm{LHV}} \quad (35)$$

Where W_{sys} is the total output power of the system, $q_{\mathrm{fuel,in}}$ is the fuel flow rate entering the system, and LHV is the lower heating value of the system fuel.

Analysis of system impact based on entropy generation and exergy analysis

To investigate the directionality of energy transfer, the entropy generation principle can be used to identify the irreversibility of thermodynamic processes. For any system, the entropy generation (S_{gen}) arises due to irreversibilities. Based on the Clausius inequality ($\oint \frac{\delta Q}{T} \leq 0$), the following expression can be derived:

$$\mathrm{ds} = \frac{\delta Q}{T} + \delta S_{gen} \quad (37)$$

Therefore, if the process within the system is irreversible, the entropy generation will be greater than zero, expressed as:

$$S_{gen} \geq 0 \quad (38)$$

Exergy is defined as the maximum useful work that a system can deliver as it undergoes a reversible process from an arbitrary state to the dead state. This section will evaluate the irreversibility of the actual process by calculating the exergy destruction of each component in the system. In general, the exergy of a fluid can be expressed as the sum of its physical and chemical exergy.

$$\dot{E}X^{tot} = \dot{E}X^{ph} + \dot{E}X^{ch} \quad (39)$$

Where:

$$\dot{E}X^{ph} = \sum_i \{\dot{m}_i[(h - h_0) - T_0(s - s_0)]\} \quad (40)$$

$$\dot{E}X^{ch} = \sum_i \dot{n}_i \sum_i \left[x_i(\overline{ex}_i^{ch,0} + RT_0 \ln(x_i)\right] \quad (41)$$

In the above expression, the subscript "0" denotes thermodynamic properties under standard conditions, and $\overline{ex}_i^{ch,0}$ represents the standard chemical exergy. The exergy balance for each component under steady-state conditions can be expressed as:

$$\dot{E}_d = \sum_j \left(1 - \frac{T_0}{T_j}\right) \dot{Q}_j - \dot{W}_{CV} + \sum_i \dot{m}_i ex_i - \sum_e \dot{m}_e ex_e \quad (42)$$

Where $\dot{E}_d$ represents the exergy destruction, ex is the specific exergy, and $\dot{Q}_j$ is the heat transfer rate. Under steady-state conditions, the exergy loss of each component can be determined through exergy calculations. The following provides the exergy calculation equations for each component in the system:

I. SOFC stack

$$\dot{E}_{d,SOFC} = \left(\dot{E}_{in,a} + \dot{E}_{in,c}\right) - \left(\dot{E}_{out,a} + \dot{E}_{out,c}\right) - W_{out,SOFC} \quad (43)$$

II. Reformer

$$\dot{E}_{d,ref} = \dot{E}_{in,ref} - \dot{E}_{out,ref} \quad (44)$$

III. Heat exchanger

$$\dot{E}_{HX} = \left(\dot{E}_{in,hot} + \dot{E}_{in,cold}\right) - \left(\dot{E}_{out,hot} + \dot{E}_{out,cold}\right) \quad (45)$$

IV. Burner

$$\dot{E}_{burner} = \dot{E}_{in} - \dot{E}_{out} \quad (46)$$

V. Compressor

$$\dot{E}_{comp} = \dot{E}_{in} - \dot{E}_{out} + W_{in,comp} \quad (47)$$

VI. Turbine

$$\dot{E}_{turb} = \dot{E}_{in} - \dot{E}_{out} - W_{out,turb} \quad (48)$$

In addition to analyzing the exergy of each component, the second law of thermodynamics can also be used to define the exergy efficiency, which is expressed as the ratio of the total electrical output of the system to the total input exergy. It can be represented as:

$$\eta_{\mathrm{II}} = \frac{\mathrm{P_{sys}}}{\dot{\mathrm{E}}\mathrm{x}_{\mathrm{in}}} \quad (49)$$

Where $\dot{\mathrm{E}}\mathrm{x}_{\mathrm{in}}$ in represents the exergy input to the system.

Internal system and external combustion engine loop design

Based on the literature review, it is evident that the SOFC system requires a reformer to prevent carbon deposition. However, within the SOFC power generation system loop, the reformer significantly affects the system's output power and efficiency. This subsection provides a detailed explanation and itemized introduction of different reformer types and their corresponding system configurations and designs. The main parameters of the system are listed in Table 2.

To effectively analyze the overall performance of the SOFC power generation system, the following key assumptions are adopted in this study:

1. All gases are assumed to behave as ideal gases.
2. The ambient temperature of the system is 298 K, and the atmospheric pressure is 1 atm.
3. Air consists of 21% oxygen and 79% nitrogen by volume.

4. The operating temperature of the cell is equal to the outlet fluid temperature.
5. Unreacted fuel is completely oxidized in the burner.

Table 2. Operating parameter of SOFC system

System	
Parameters	Value
Operating pressure [bar]	1-5
Fuel molar flow rate [mol/s]	0.0244
Air molar flow rate [mol/s]	0.8784
Steam to carbon ratio [-]	1.8
Oxygen to carbon ratio [-]	0.1
heat exchanger effectiveness [%]	80-87%
combustion efficiency [%]	100%

Reformer loop design of the SOFC power generation system

According to the previous literature review, the use of a reformer is essential in SOFC systems to prevent carbon deposition. However, within the SOFC power generation system loop, the reformer significantly affects the system's output power and efficiency. This subsection provides a detailed explanation and itemized introduction of various reformer types, along with their corresponding system loop designs and configurations.

Steam reforming

The steam reforming reaction between steam and fuel typically employs materials such as nickel or noble metals, with the primary control parameter being the steam-to-carbon ratio (S/C). This reaction is highly endothermic. Sufficient heat must be supplied to the reforming gases to sustain the reaction, as represented by equations (29) and (30). Although steam reforming can achieve a higher methane conversion rate, it requires a relatively large heat input. Therefore, the system loop and component design must be scaled accordingly, resulting in longer startup times.

Partial oxidation reforming

The catalyst materials for partial oxidation reforming are typically platinum or copper. This process involves the reforming reaction between oxygen and fuel, with the air (oxygen)/fuel ratio serving as the primary control parameter. As an exothermic reaction, it generates heat during the reforming process, which helps raise the temperature of the gas exiting the reformer to the level required by the fuel cell stack. Compared to steam reforming, the system loop design is significantly simpler. However, the methane conversion rate is considerably lower, resulting in reduced output power from the stack. The chemical reaction is represented by equation (31).

Autothermal reforming

By combining steam reforming and partial oxidation reforming reactions, steam, oxygen, and fuel are simultaneously introduced into the reformer for reaction. The mechanism involves an initial exothermic partial oxidation reaction between the fuel and oxygen, which generates thermal energy for the subsequent endothermic reaction with steam. This approach enhances methane conversion while integrating the advantages of both reforming methods—namely, the high methane conversion rate of steam reforming and the simplified system loop design of partial oxidation reforming.

This study investigates the power generation performance of SOFC systems employing different reformers through a simplified system loop design, as illustrated in Fig. 1.

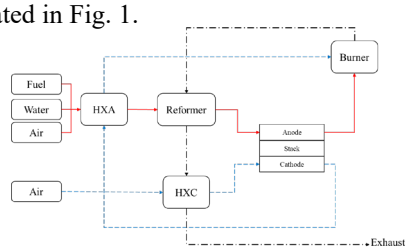

Figure 1. Schematic diagram of the SOFC power generation system

Loop design and efficiency calculation of SOFC integrated with external combustion engine

Due to the high-temperature exhaust gases produced by the SOFC system, numerous studies have proposed integrating SOFC power systems with external combustion engines to form hybrid power generation cycles, thereby enhancing system output power and overall efficiency. Currently, the most commonly integrated external combustion engines with SOFC systems include gas turbines, organic Rankine cycle systems, and Stirling engines. Based on the results of the preceding reformer analysis, the most advantageous reforming system is selected for subsequent research and analysis in this study. The power calculation formulas and system configurations of each external combustion engine are illustrated in Figs. 2 to 4.

Gas turbine

The compressor (c) and gas turbine (g) operate under isentropic processes, and the work performed can be expressed as (Park and Kim 2006):

$$W_c = \frac{kRT_{in}}{k-1}\left[\left(\frac{P_{out}}{P_{in}}\right)^{\frac{k-1}{k}} - 1\right] \quad (50)$$

$$W_g = \frac{kRT_{in}\eta_t}{k-1}\left[\left(\frac{P_{out}}{P_{in}}\right)^{\frac{k-1}{k}} - 1\right] = \frac{kR}{k-1}(T_{out} - T_{in}) \quad (51)$$

where k is the adiabatic index and η_t represents the gas turbine efficiency.

The system configuration of the SOFC-GT is illustrated in Fig. 2, and the overall electrical efficiency is calculated using the following equation:

$$\eta_{I,el} = \frac{W_{SOFC}+W_g-W_c-W_{in}}{q_{fuel,in}\times LHV} \quad (52)$$

$$\eta_{I,th} = \frac{W_{turb}}{q_{fuel,in} \times LHV} \quad (53)$$

Where W_{SOFC} denotes the total output power of the SOFC system, $q_{fuel,in}$ is the fuel flow rate entering the system, LHV represents the lower heating value of the fuel, W_{turb} is the power output of the turbine recovered from system heat, and W_{in} is the input power to the system.

Organic Rankine Cycle

The work output of the steam turbine can be expressed as (Akkaya and Sahin 2009):

$$W_{ST} = m_{st}(h_{st,out} - h_{st,in})\eta_{st} \quad (54)$$

Where W_{ST} is the output power of the steam turbine, m_{st} is the mass flow rate in the ORC system, h denotes specific enthalpy, and η_{st} represents the steam turbine efficiency.

The system configuration of the SOFC-ORC is illustrated in Fig. 3, and the overall electrical efficiency is calculated using the following equation:

$$\eta_{I,el} = \frac{W_{SOFC}+W_{ST}}{q_{fuel,in} \times LHV} \quad (55)$$

$$\eta_{I,th} = \frac{W_{ST}}{q_{fuel,in} \times LHV} \quad (56)$$

Stirling engine

The power output of the Stirling engine ($W_{Stirling}$) is calculated using the following equation (Hosseinpour et al. 2017):

$$W_{Stirling} = \eta_{Stirling}(Q_{high} - Q_{loss}) \quad (57)$$

$$\eta_{Stirling} = \frac{[(1-CR^{1-r})-TR(CR^{r-1}-1)]}{[(1-CR^{1-r})-(1-TR)(1-\varepsilon_r)]} \quad (58)$$

Where $\eta_{Stirling}$ is the efficiency of the Stirling engine, Q_{high} is the input heat to the engine, Q_{loss} is the heat loss rate, CR is the compression ratio, r is the specific heat ratio, and ε_r is the regenerator efficiency.

The system configuration of the SOFC-SE is illustrated in Fig. 4, and the overall electrical efficiency is calculated using the following equation:

$$\eta_{I,el} = \frac{W_{SOFC}+W_{Stirling}}{q_{fuel,in} \times LHV} \quad (59)$$

$$\eta_{I,th} = \frac{W_{Stirling}}{q_{fuel,in} \times LHV} \quad (60)$$

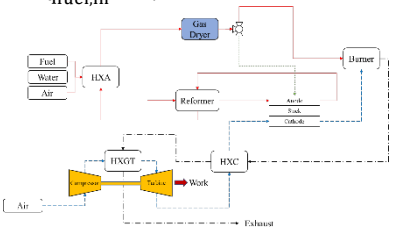

Figure 2. Schematic diagram of SOFC-GT system loop

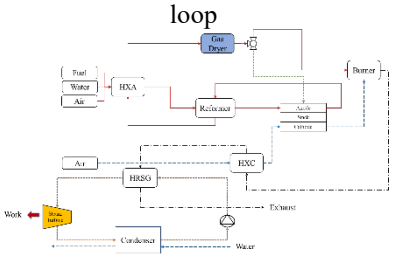

Figure 3. Schematic diagram of SOFC-ORC system loop

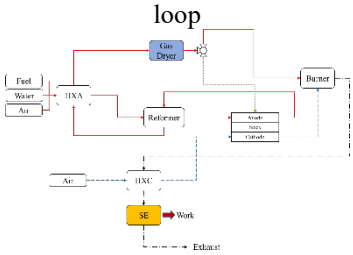

Figure 4. Schematic diagram of SOFC-SE system loop

Results and discussion

Performance and efficiency analysis of the SOFC stack

Based on the SOFC operating parameters listed in Table 1, simulations were conducted at operating temperatures of 973 K, 1023 K, and 1073 K. The results were overlaid for comparison to generate the current density–voltage curve and current density–power density curve. As shown in Fig. 5, both the cell voltage and power density increase with rising temperature. The fuel cell stack used in the subsequent system will follow the performance trend of this single cell.

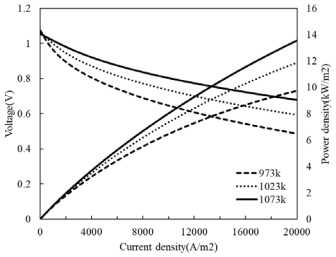

Figure 5. Performance curve of the SOFC stack

Efficiency enhancement of the SOFC through reformer and system parameters

Figs. 6 to 8 illustrate the temperature distribution of each component in the system under the operation of three different reformers. As predicted in Section above, the average SOFC stack temperature is approximately 977.96 K for the SR reforming system, around 1013.69 K for the ATR reforming system, and reaches up to 1080.88 K in the POx reforming system. In addition, the micro-combustor, which serves as the primary heat source in the SOFC system, utilizes the unreacted fuel from the SOFC stack for combustion, thereby generating high-temperature heat that is recovered to preheat the incoming fuel. Therefore, as the fuel utilization rate in the stack increases, the overall system temperature decreases, with the most significant temperature drop observed at the combustor outlet.

Figs. 9 and 10 present the effects of fuel utilization rate on system output power and efficiency. Stack temperature is identified as the key factor influencing power output; higher temperatures lead to increased power density. Given that the hydrogen production capacities of ATR and SR systems are

comparable, the higher system temperature achieved by ATR enables greater power output and efficiency than SR. However, despite the higher SOFC stack temperature observed in the POx system compared to the other two reforming systems, its lower hydrogen production efficiency results in reduced system performance. In addition to modifying the reformer loop, increasing the fuel utilization rate of the stack also enhances system output power and efficiency.

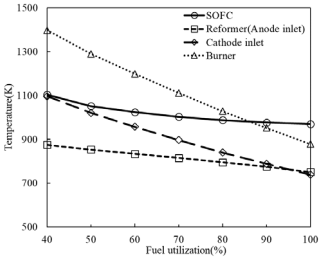

Figure 6. Effect of fuel utilization on the temperature of each component in the ATR+SOFC system

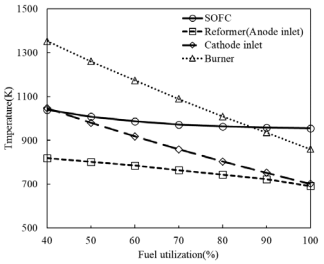

Figure 7. Effect of fuel utilization on the temperature of each component in the SR+SOFC system

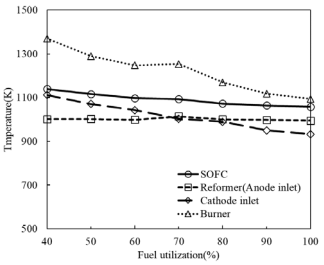

Figure 8. Effect of fuel utilization on the temperature of each component in the POx+SOFC system

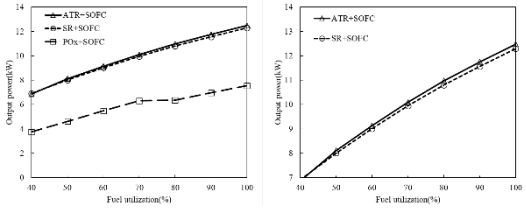

Figure 9. Effect of fuel utilization on stack output power in different reforming systems

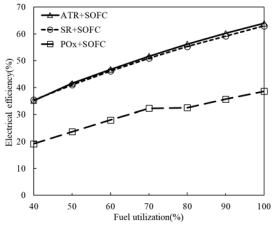

Figure 10. Effect of fuel utilization on power generation efficiency in different reforming systems

Thermoelectric efficiency enhancement of the SOFC hybrid power generation system

Figs. 11 to 13 show that as the fuel utilization rate in the SOFC stack increases, the temperatures of various components in the system decrease. This trend may be attributed to the reduction of unreacted fuel entering the combustor at higher fuel utilization rates; with less residual fuel available for combustion, the combustor temperature drops accordingly. As observed from the system diagrams, the cathode air entering the SOFC stack is primarily heated by the exhaust gas from the combustor. Consequently, the cathode inlet temperature also decreases with increasing fuel utilization rate. In contrast, the temperature at the anode inlet is not significantly affected by changes in fuel utilization.

As the SOFC fuel utilization rate increases, more fuel is directly used for power generation within the stack, which serves as the primary power-generating component of the system. Therefore, in SOFC-GT, SOFC-ORC, and SOFC-SE systems, the SOFC power output, total system output power, and overall electrical efficiency all increase with higher fuel utilization. However, since more fuel is consumed within the SOFC stack, less thermal energy remains available for the external combustion engines, leading to a decrease in their power output and thermal efficiency.

Among the three configurations, the SOFC-SE system exhibits a higher overall system efficiency compared to SOFC-GT and SOFC-ORC. Figs. 14 to 16 illustrate the distributions of output power and efficiency for SOFC-GT, SOFC-ORC, and SOFC-SE systems, respectively, as the fuel utilization rate increases from 40% to 100%. A comparative summary of the output power for the three hybrid systems is also provided in Table 3.

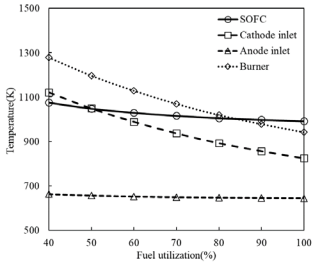

Figure 11. Effect of fuel utilization on the temperature of each component in the SOFC-GT system

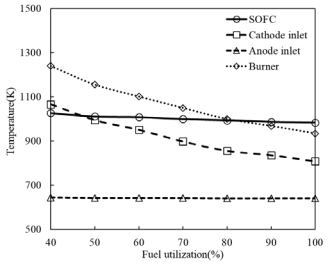

Figure 12. Effect of fuel utilization on the temperature of each component in the SOFC-ORC

system

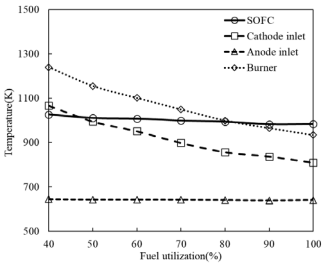

Figure 13. Effect of fuel utilization on the temperature of each component in the SOFC-SE system

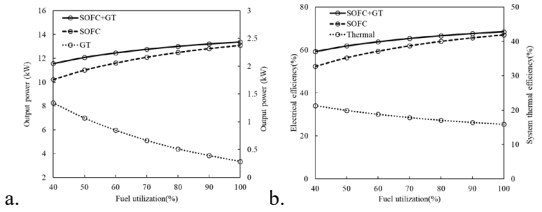

Figure 14. Effect of fuel utilization on (a) output power and (b) thermoelectric efficiency of the SOFC-GT system

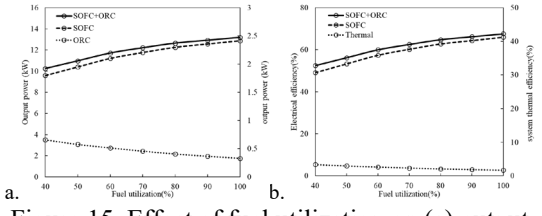

Figure 15. Effect of fuel utilization on (a) output power and (b) thermoelectric efficiency of the SOFC-ORC system

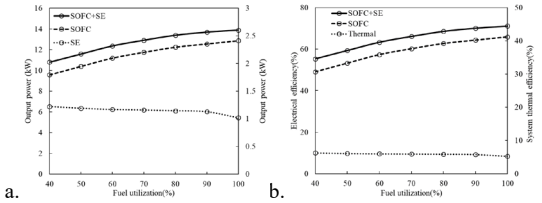

Figure 16. Effect of fuel utilization on (a) output power and (b) thermoelectric efficiency of the SOFC-SE system

Table 3. Effect of FU on the output power of the hybrid power generation system

FU [%]	GT	ORC	SE
	Output power [kW]		
40	11.57	10.23	10.80
50	12.08	10.97	11.58
60	12.46	11.71	12.36
70	12.76	12.21	12.91
80	13.01	12.65	13.39
90	13.21	12.81	13.58
100	13.38	13.19	13.89

Exergy efficiency and entropy generation analysis of each component in the SOFC hybrid power generation system

By applying the principles of entropy generation and exergy efficiency calculations, different system configurations and optimized operations can be employed to reduce exergy losses and enhance overall system efficiency. Using the equations presented in Section above, the entropy generation and exergy efficiency of each system component are calculated to identify the sources of energy loss. The analysis is conducted under a fixed fuel flow rate at the system inlet to investigate variations in component entropy generation and overall exergy efficiency.

As shown in Fig. 17, the HXC component exhibits the highest entropy generation, primarily due to the large temperature gradient between the high-temperature gas produced by the combustor and the ambient-temperature cathode air involved in the heat exchange process. Additionally, the ORC system demonstrates higher energy losses compared to the GT and SE systems, indicating that the SOFC-ORC system has relatively lower exergy availability, as illustrated in Fig. 18. A comparative summary of thermal efficiency and exergy efficiency across the three hybrid systems with different external combustion engines is provided in Table 4.

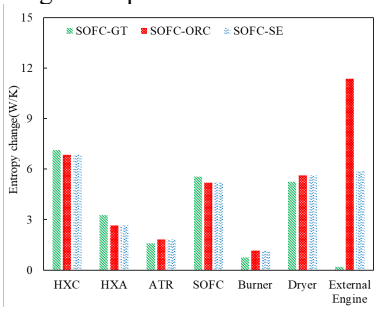

Figure 17. Entropy generation of major components in each system

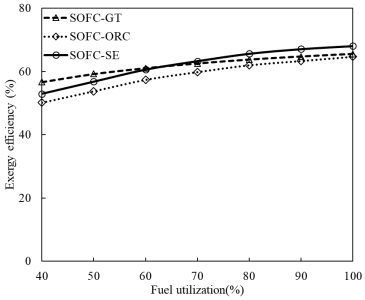

Figure 18. Effect of FU on the exergy efficiency of each system

Table 4. Effect of FU on thermoelectric efficiency and exergy efficiency of the hybrid power generation system

FU	GT	ORC	SE

[%]	η_{el} [%]	η_{th} [%]	η_{ex} [%]	η_{el} [%]	η_{th} [%]	η_{ex} [%]	η_{el} [%]	η_{th} [%]	η_{ex} [%]
40	59.3	21.3	56.7	52.4	3.4	50.1	55.3	6.3	52.9
50	61.9	19.9	59.2	56.2	3.0	53.7	59.3	6.1	56.8
60	63.8	18.8	61.0	56.0	2.6	57.4	63.3	6.0	60.6
70	65.4	17.9	62.5	62.5	2.3	59.8	66.1	5.9	63.3
80	66.7	17.1	63.8	64.8	2.1	61.7	68.6	5.9	65.6
90	67.8	16.5	64.7	65.6	1.9	63.3	70.1	5.8	67.1
100	68.0	15.9	65.53	67.6	1.68	64.64	71.13	5.22	68.03

Conclusion

The study confirms that, under appropriate loop design and operating parameters, the ATR reformer achieves higher system efficiency compared to SR and POx reformers. This is primarily because the ATR reformer enables a higher stack temperature, allowing higher-temperature fuel to enter the SOFC stack relative to the SR system. Furthermore, simulation results, along with exergy efficiency and component-wise entropy generation analysis, reveal that the SOFC-SE system exhibits the highest overall efficiency. The entropy generation analysis also indicates that the SOFC-ORC system experiences greater entropy generation across its components, leading to comparatively lower system efficiency.

Acknowledgement

The continuous financial support from the National Science and Technology Council in Taiwan is greatly acknowledged.

References

Akkaya, A. V., & Sahin, B. (2009). A study on performance of solid oxide fuel cell-organic Rankine cycle combined system. International Journal of Energy Research, 33(6), 553–564.

Aguiar, P., Adjiman, C. S., & Brandon, N. P. (2004). Anode-supported intermediate temperature direct internal reforming solid oxide fuel cell. I: Model-based steady-state performance. Journal of Power Sources, 138(1–2), 120–136.

Bae, G., Bae, J., Kim-Lohsoontorn, P., & Jeong, J. (2010). Performance of SOFC coupled with n-C4H10 autothermal reformer: Carbon deposition and development of anode structure. International Journal of Hydrogen Energy, 35(22), 12346–12358.

Carapellucci, R., & Giordano, L. (2020). Steam, dry and autothermal methane reforming for hydrogen production: A thermodynamic equilibrium analysis. Journal of Power Sources, 469, 228391.

Duc, N., & Fujit, G. (2012). Modelling a SOFC power unit using natural gas fed directly. In Advances in Natural Gas Technology (Chapter 13).

Hosseinpour, J., Sadeghi, M., Chitsaz, A., Ranjbar, F., & Rosen, M. A. (2017). Exergy assessment and optimization of a cogeneration system based on a solid oxide fuel cell integrated with a Stirling engine. Energy Conversion and Management, 143, 448–458.

Liso, V., Olesen, A. C., Nielsen, M. P., & Kær, S. K. (2011). Performance comparison between partial oxidation and methane steam reforming processes for solid oxide fuel cell (SOFC) micro combined heat and power (CHP) system. Energy, 36(7), 4216–4226.

Lai, H. Y., Lin, H. J., & Chan, Y. H. (2025). Efficiency enhancement on solid oxide fuel cell system with anode off-gas recycle by evaluating entropy and exergy change. Journal of Power Sources Advances, 32, 100172

Li, Y., Wang, Y., Zhang, X., & Mi, Z. (2008). Thermodynamic analysis of autothermal steam and CO_2 reforming of methane. International Journal of Hydrogen Energy, 33(10), 2507–2514.

Noponen, M., Torri, P., Göös, J., Chade, D., Hallanoro, P., Temmo, A., Koit, A., & Õunpuu, E. (2015). Status of solid oxide fuel cell development at Elcogen. ECS Transactions, 28(1), 151–156.

Park, S. K., & Kim, T. S. (2006). Comparison between pressurized design and ambient pressure design of hybrid solid oxide fuel cell–gas turbine systems. Journal of Power Sources, 163(1), 490–499.

Rabenstein, G., & Hacker, V. (2008). Hydrogen for fuel cells from ethanol by steam-reforming, partial-oxidation and combined auto-thermal reforming: A thermodynamic analysis. Journal of Power Sources, 185(2), 1293–1304.

Somekawa, T., Nakamura, K., Kushi, T., Kume, T., Fujita, K., & Yakabe, H. (2017). Examination of a high-efficiency solid oxide fuel cell system that reuses exhaust gas. Applied Thermal Engineering, 114, 1387–1392.

Vrečko, D., Nerat, M., Vrančić, D., Dolanc, G., Dolenc, B., Pregelj, B., Meyer, Au, S.F., Makkus, R., Juričić, Đ., (2018). Feedforward-feedback control of a solid oxide fuel cell power system. International Journal of Hydrogen Energy, 43(12), 6352–6363.

Vita, A., Pino, L., Italiano, C., & Palella, A. (2019). Steam reforming, partial oxidation, and autothermal reforming of ethanol for hydrogen production in conventional reactors. In Ethanol (pp. 159–191).